Biosensors and Bioelectronics 135 (2019) 173–180

Contents lists available at ScienceDirect

Biosensors and Bioelectronics

journal homepage: www.elsevier.com/locate/bios

Ultrabright fluorescent microsphere and its novel application for improving the sensitivity of immunochromatographic assay

Gang-gang Zhang, Shao-lan Xu, Yong-hua Xiong, Hong Duan, Wen-yao Chen, Xiang-min Li, Mei-fang Yuan, Wei-hua Lai*

State Key Laboratory of Food Science and Technology, Nanchang University, Nanchang, 330047, China

ARTICLE INFO

Keywords:
Aggregation-induced emission
Fluorescent microsphere
Escherichia coli O157:H7
Immunochromatographic assay

ABSTRACT

Fluorescent microsphere (FM) is widely used as probe in immunochromatographic assay (ICA). However, the performance of conventional FM is limited because of the aggregation-caused quenching effect. Herein, we compared a kind of conventional FM (DMFFM, loading DMF) with novel aggregation-induced emission FM (AIEFM, loading TCBPE). The fluorescence intensity of DMFFM initially increased and then decreased as the concentrations of the loading DMF increased. The fluorescence intensity of AIEFM increased as the concentrations of the loading TCBPE increased and retained a high value. AIEFM was compared with two commercial FMs purchased from Ocean (OFM) and Merk (MFM). The maximum fluorescence intensity and relative quantum yield of AIEFM was approximately 5 and 4.5 times higher than those of two commercial FMs. We used the novel AIEFM as a probe to improve the sensitivity of ICA. When *Escherichia coli* O157:H7 was detected as the target, the limit of detection of ICA based on AIEFM, OFM and MFM were 3.98×10^3 CFU/mL, 4.48×10^4 and 2.78×10^4 CFU/mL, respectively. The ICA of AIEFM had 11 and 7 times improvement in sensitivity compared with that of OFM and MFM. Our results could be used as a basis for novel probes in practical ICA applications.

1. Introduction

Immunochromatographic assay (ICA) is widely used in food safety (Zhou et al., 2014; Wang et al., 2016; Duan et al., 2017; Li et al., 2018), environmental monitoring (Qiao et al., 2018; Xiao et al., 2017; Wu et al., 2017; Ouyang et al., 2018), and clinical diagnosis (Wang et al., 2015; Feng et al., 2014; Loynachan et al., 2018; Hu et al., 2013) because of its convenience, rapidity, and low cost (Parolo and Merkoci, 2013). The probe is the key part of this assay (Shan et al., 2015). Gold nanoparticles (Chen et al., 2017; Kong et al., 2016) and conventional fluorescent microspheres (FMs), such as organic dye FM (Lou et al., 2018; Liu et al., 2015), quantum dot microsphere (Ren et al., 2014; Shao et al., 2018), upconversion FM (You et al., 2017; He et al., 2018a), and time-resolved FM (Hu et al., 2017; Tang et al., 2017), are commonly used in ICA. FMs have lower background and higher signal than gold nanoparticles in terms of absorbance when they are applied to ICA (Xie et al., 2014).

The fluorescence intensity of conventional FMs, which have different concentrations of loading fluorescent materials (Qiu et al., 2015), is the core performance used for their utilization as a probe in ICA (Gong et al., 2017). However, the loading amount of FMs is limited because of the aggregation-caused quenching (ACQ) (Huang et al., 2016; Fu et al., 2015) effect of conventional fluorescent materials, and their optical performance is poor (Reisch and Klymchenko, 2016), resulting in the low sensitivity of ICA.

A novel class of luminescent dyes with aggregation-induced emission (AIE) (Zhao et al., 2015) has been developed to overcome the ACQ problem (Chen et al., 2015). The AIE process may be associated with the restriction of intramolecular rotation (Chen et al., 2003; Yang et al., 2016), J-aggregate formation (Kim et al., 2015), twisted intramolecular charge transfer (Lu et al., 2016), and excited-state intramolecular proton transfer (He et al., 2018b). The important feature of AIE dyes is that aggregates are more brilliant than individuals (Mei et al., 2014). Thus, the absorbance and brightness of aggregation-induced emission fluorescent microspheres (AIEFM), which are resistant to concentration quenching, can be enhanced by increasing the amount of loading dye until AIEFMs are entirely made of pure dyes. Therefore, AIE dyes and AIEFMs have been widely used in bioimaging (Li et al., 2017; Chen et al., 2016; Yan et al., 2016) and light emitting diodes (Maji et al., 2017; Liu et al., 2016; Nie et al., 2018), which require high brightness and high concentrations of optically active materials.

In this work, a novel AIEFM was synthesized via a one-pot method

* Corresponding author.
E-mail address: talktolaiwh@163.com (W.-h. Lai).

https://doi.org/10.1016/j.bios.2019.04.023
Received 8 February 2019; Received in revised form 8 April 2019; Accepted 11 April 2019
Available online 17 April 2019
0956-5663/

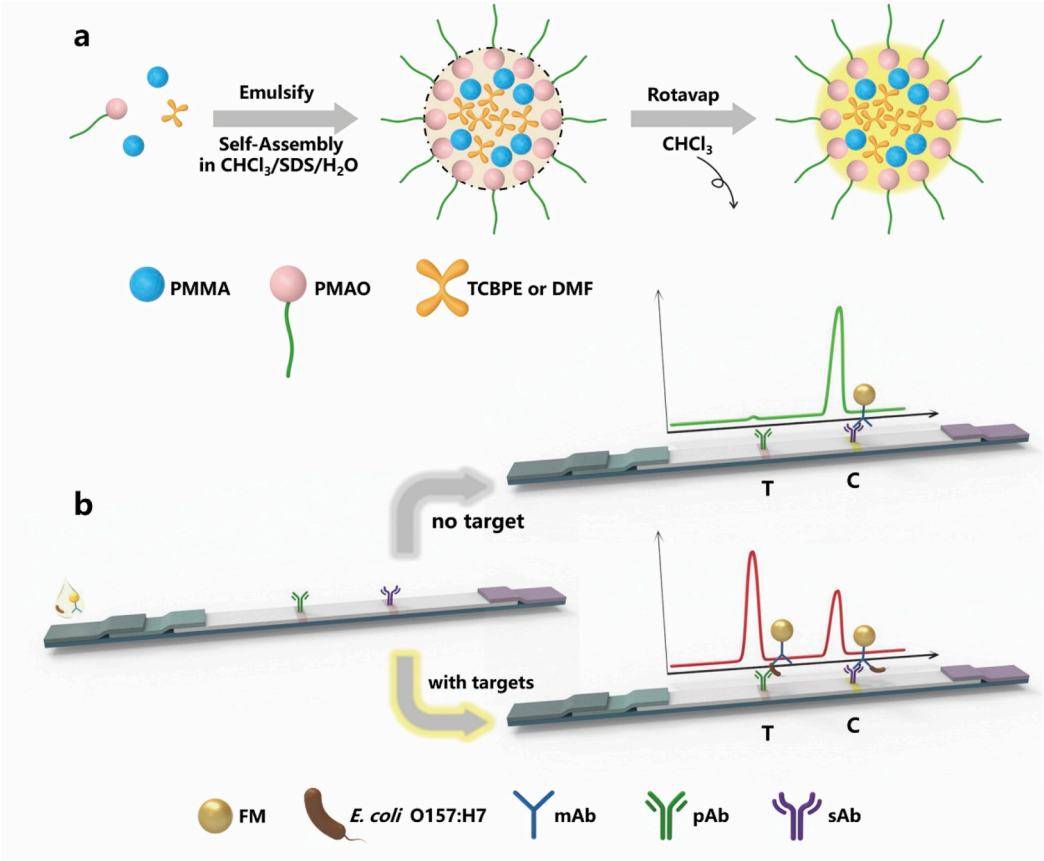

Fig. 1. Scheme of this work. One-pot synthesis strategy (a) and the principle of ICA based on AIEFM (b).

(Fig. 1a) (Chen et al., 2011). Poly(methyl methacrylate) (PMMA), poly (maleic anhydride-*alt*-1-octadecene) (PMAO), sodium dodecyl sulfate (SDS), and tetramethyl 4′,4‴,4⁗,4⁗′-(ethene-1,1,2,2-tetrayl) tetrakis([1,1′-biphenyl]-4-carboxylate) (TCBPE) were used as polymer framework, functional linker, surfactant, and loading dye, respectively. The TCBPE, PMMA, and PMAO are solid compounds. They can be dissolved in chloroform. The mixture formed oil-in-water nanoemulsions which loading controllable concentration of dye under high power ultrasonication. The hydrophilic end of PMAO as functional group was outward under the force of hydrophobic interaction. After evaporating organic solvent by rotary evaporator, TCBPE-oil form was converted into solid microsphere stably embedded the fluorescent dyes. In this method, high loading and rich functionalization were completed in one step.

Ultrabright AIEFM was utilized to detect *Escherichia coli* O157:H7 (*E. coli* O157:H7, ATCC 43888) in ICA (Fig. 1b). AIEFM-labeled anti-*E. coli* O157:H7 monoclonal antibody was used as a probe (AIEFM-mAb). Anti-*E. coli* O157:H7 polyclonal antibody (pAb) and goat anti-mouse antibody (sAb) were immobilized on the nitrocellulose membrane through hydrophobic-hydrophobic interactions (Bishnoi et al., 2011) as the test line (T line) and the control line (C line), respectively. The AIEFM-mAb-*E. coli* O157:H7 complex was formed and captured by anti-*E. coli* O157:H7 pAb in the presence of *E. coli* O157:H7 in the sample, generating a fluorescent signal on the T line. In ICA, *E. coli* O157:H7 could be rapidly and specifically detected.

2. Materials and methods

2.1. Materials

E. coli O157:H7 strain ATCC 43888 was cultured in a Luria–Bertani medium (LB; Oxoid, Basingstoke, UK) at 37 °C for 20 h before use. *Salmonella choleraesuis* (*S. choleraesuis*), *Listeria monocytogenes* (*L. monocytogenes*), *Shigella*, *Staphylococcus aureus* (*S. aureus*), *Escherichia coli* (*E. coli*), *E. coli* O157:H7 48, and *E. coli* O157:H7 54 were obtained from Jiangxi CDC. Tetramethyl 4′,4‴,4⁗,4⁗′-(ethene-1,1,2,2-tetrayl) tetrakis([1,1′-biphenyl]-4-carboxylate) (TCBPE, the chemical structure is shown in Fig. S1b) was custom made by Da Yang (Xuzhou Da Yang Biochemical Technology Co., Ltd., China). Fluorescein, Poly(methyl methacrylate) (PMMA), and Sodium dodecyl sulfate (SDS) were obtained from Aladdin (Shanghai Aladdin Bio-Chem Technology Co., Ltd., China). Poly(maleic anhydride-*alt*-1-octadecene) (PMAO), dimethyl sulfate, 1-ethyl-3-(3-dimethylaminopropyl) carbodiimide (EDC), N-hydroxysulfosuccinimide sodium salt (NHSS), casein, phosphate buffer saline (PBS, 0.01 M, pH = 7.4), bovine serum albumin (BSA), and boric acid buffer (BB, 0.2 M, pH = 8) were purchased from Sigma-Aldrich (Merck KGaA, Germany). Carboxylated fluorescent microsphere (size: 0.167 μm, Ex/Em: 470 nm/525 nm, 10 mg/mL) was obtained from Ocean (Ocean NanoTech, US). Latex Calibrated fluorescent microsphere (size: 0.175 μm, Ex/Em: 470 nm/525 nm, 10 mg/mL) was purchased from Estapor (Merck KGaA, Germany). Anti-*E. coli* O157:H7 monoclonal antibody (mAb; Catalog #: C65110M) and rabbit anti-*E. coli* O157:H7 polyclonal antibody (pAb; Catalog #: B65001R) were procured from Meridian Life Science, Inc. (Memphis, TN). The sample pad, the nitrocellulose membrane, and the absorbent pad were purchased from Millipore, Inc. (Bedford, MA). All of the solvents and other chemicals were of analytical reagent grade.

2.2. Equipment

The ultrasonic processor (FS-600N) was acquired from Shanghai Sonxi Ultrasonic Instrument Co., Ltd. (China). The BioDot XYZ platform, which combined motion control with BioJet Quanti3050k and AirJet Quanti3050k dispensers, was acquired from BioDot (Irvine, CA).

Fluorescent intensity strip readers ($\lambda_{emission}$ = 525 nm, $\lambda_{excitation}$ = 365 nm or 470 nm) were obtained from Hangzhou Hemai Technology Co., Ltd. (China). Biosafety cabinet (BHC-1300 II A/B_3) was acquired from Airtech (Suzhou Antai Airtech Co., Ltd., China).

2.3. Synthesis of dimethylated fluorescein (DMF)

In brief, fluorescein (6.6 g) and K_2CO_3 (11 g, 4 eq) were mixed with acetone (50 mL) at room temperature and vigorously stirred for 10 min. Dimethyl sulfate (2.3 mL) was added dropwise in the mixture in an ice bath. The mixture was stirred for 1 h at room temperature and refluxed overnight at 50 °C. After the reaction was completed, NaOH (10 mL, 1 M) was added for the quenching reaction. The solution was washed with water and ethyl acetate. After evaporating, the reddish-brown product was obtained. The reaction equation is shown in Fig. S1a.

2.4. Synthesis of TCBPE fluorescent microsphere (AIEFM) and DMF fluorescent microsphere (DMFFM)

The AIEFM was obtained on the basis of the following steps. TCBPE was added to PMMA/PMAO chloroform stock solution (PMMA: 50 mg/mL; PMAO: 25 mg/mL) at a series of final concentrations of 0, 2, 5, 12.5, 20, 30, 40, and 50 mg/mL. Then, 240 μL of the TCBPE solution was added to 1.2 mL of the SDS aqueous solution (0.25%, w/w). In an ice bath, the emulsion was emulsified for 3 min by using an ultrasonic processor at power of 120 W. Subsequently, the chloroform was removed by using a rotavapor, and the mixture was centrifuged at 12,000 r/min at 4 °C for 20 min. The supernatant was saved and considered as first-step supernatant. The resulting precipitate was washed with NaOH (0.01 M) thrice. Finally, the precipitate was redissolved in 1.8 mL of BB (0.2 M, pH = 8) and stored at 4 °C in the dark. DMFFM was obtained by using the same method with DMF as a fluorescent dye.

The different-sized FMs were synthesized by adjusting the power of ultrasonic processor to 60 W, 120 W, and 180 W. The concentrations of DMF and TCBPE were 20 and 30 mg/mL, respectively. The other steps were the same as above.

2.5. Quantification of residual TCBPE and DMF in first-step supernatant

The first-step supernatant was diluted with NaOH (0.01 M) to a total volume of 3 mL. The mixture was extracted with ethyl acetate (3 mL × 4). The combined organic layers were evaporated, and the products were weighted.

2.6. Preparation of AIEFM-mAb, OFM-mAb, and MFM-mAb

The carboxyl group on the surface of AIEFM was activated for linking AIEFM and anti-*E. coli* O157:H7 mAb. AIEFM (20 μL, 10 mg/mL) was dispersed in 2 mL of BB (0.2 M, pH 8.0). Then, 40 μL of EDC (10 mg/mL, freshly prepared) and 30 μL of NHSS (10 mg/mL, freshly prepared) were added to the mixture and stirred for 2 h in the dark. The resulting solution was centrifuged at 10,000 r/min at 4 °C for 20 min. The supernatant was discarded, and the resultant precipitate was washed with water twice. The activated AIEFM was redissolved in 2 mL of BB (0.2 M, pH 8.0). The activated MFM and the activated OFM were obtained by using the same method.

AIEFM-mAb formation was conducted as follows. Anti-*E. coli* O157:H7 mAb solution (0.2 mL, 100 μg/mL) was added to the activated AIEFM (2 mL, 0.1 mg/mL) dropwise with gentle stirring for 60 min. Then, 0.2 mL of casein (1% wt/vol) was added to block in the dark for 0.5 h. The resulting solution was centrifuged at 8500 r/min at 4 °C for 20 min. The supernatant was discarded to remove the unreacted free antibody, and the resultant precipitate was redissolved in 200 μL of dilution buffer. MFM-mAb and OFM-mAb were obtained by using the same method.

2.7. Preparation of the immunochromatographic test strips

Anti-*E. coli* O157:H7 pAb and sAb were diluted with PBS (0.01 M) to the final concentrations of 1.0 and 0.6 mg/mL, respectively. The two mixtures were applied to test (T) and control lines (C) on the nitrocellulose membrane and dried at 30 °C overnight. The nitrocellulose membrane, the conjugate pad, the absorption pad, and the pretreated sample pad were assembled as the test strip (Fig. S2).

2.8. Detection of E. coli O157:H7 in ICA

PBS was spiked with *E. coli* O157:H7 at concentrations of 0, 1×10^2, 5×10^2, 1×10^3, 5×10^3,1×10^4, 5×10^4,1×10^5, 5×10^5,1×10^6, 5×10^6, and 1×10^7 CFU/mL. A total of 100 μL of the solution was added to an ELISA plate well in which 6 μL AIEFM-mAb, OFM-mAb, or MFM-mAb was added. After 5 min of incubation, the mixture was added to the sample pad of the test strip. After 20 min, the test strips were read by using fluorescent intensity strip readers. A calibration curve was constructed by plotting the fluorescent intensity of T as the ordinate (Y) and the concentration of *E. coli* O157:H7 as the abscissa (X). The information on the linear regression equation was established for quantitative analysis.

2.9. Specificity experiments

The specificity experiments of AIEFM-ICA were conducted as follows. PBS was spiked with *S. choleraesuis*, *L. monocytogenes*, *Shigella*, *S. aureus*, *E. coli*, *E. coli* O157:H7 48, and *E. coli* O157:H7 54 at 1×10^6 CFU/mL. The seven locale isolate strains were obtained from Jiangxi CDC. The spiked strains were detected through ICA.

3. Results and discussion

3.1. Synthesis of two uniformly sized FMs

Conventional dimethylated fluorescein (DMF) was prepared to determine the advantage of AIE. Two phenolic hydroxyl groups of fluorescein were methylated with the attack of dimethylsulfate (Fig. S1a) (Haruo et al., 1986), thereby altering *m/z* from 332 to 345 and 360 (Fig. S3). TCBPE was custom made, and its chemical structure is shown in Fig. S1b. The fluorescence spectra of the two dyes are shown in Fig. S1c (DMF: $\lambda_{emission}$ = 525 nm, $\lambda_{excitation}$ = 470 nm) and Fig. S1d (TCBPE: $\lambda_{emission}$ = 502 nm, $\lambda_{excitation}$ = 364 nm). The digital photos of the two dyes under the natural light and UV light are shown in Fig. S1e.

Subsequently, two kinds of uniformly sized FMs were synthesized, and the difference in AIEFM and DMFFMs was compared at different dye concentrations. AIEFM and DMFFM had similar hydration size (160–170 nm) and same concentrations of PMMA, PMAO, and SDS (Fig. 2a). The two FMs synthesized via a one-pot microemulsion technique were uniform because of the good controllability and stability of microemulsion. In Fig. 2a, the particle distribution index (PDI) was less than 0.055, indicating the narrow particle size distribution of the two FMs. TEM showed that the real sizes of AIEFM and DMFFM were 100 and 95 nm, respectively (Fig. 2c and d). In Fig. 2b, the absorbance of the two FMs increased as the concentration of the two dyes in the two FMs increased.

To determine how much dye molecules were loaded in single FM, the quantitative study about the number of dye molecules encapsulated in microsphere formulation was carried out. The number of dye molecules encapsulated in single FM could be calculated by equations 6 and 7 (Supplementary Material). The results were shown in Table S1. The number of dye molecules in single DMFFM at 2 (D2), 5 (D5), 12.5 (D12.5), 20 (D20), 25 (D25), 30 (D30), 40 (D40), and 50 mg/mL (D50) of DMF were 1.83×10^4, 4.66×10^4, 8.85×10^4, 1.30×10^5, 1.71×10^5, 2.10×10^5, and 2.19×10^5, respectively. The number of dye molecules in single AIEFM 2 (T2), 5 (T5), 12.5 (T12.5), 20 (T20),

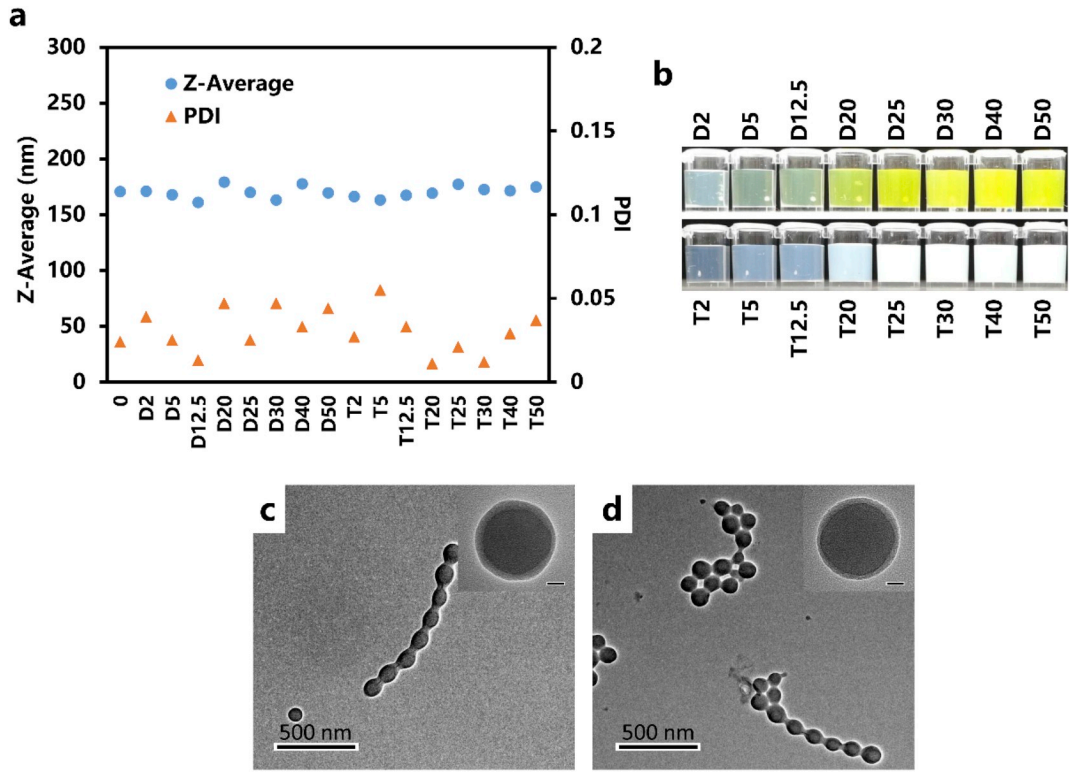

Fig. 2. Particle size characterization of FMs (0, without DMF or TCBPE; D2, 2 mg/mL DMF; D5, 5 mg/mL DMF; D12.5, 12.5 mg/mL DMF; D20, 20 mg/mL DMF; D25, 25 mg/mL DMF; D30, 30 mg/mL DMF; D40, 40 mg/mL DMF; D50, 50 mg/mL DMF; T2, 2 mg/mL TCBPE; T5, 5 mg/mL TCBPE; T12.5, 12.5 mg/mL TCBPE; T20, 20 mg/mL TCBPE; T25, 25 mg/mL TCBPE; T30, 30 mg/mL TCBPE; T40, 40 mg/mL TCBPE; T50, 50 mg/mL TCBPE). (a) is the hydration size images of FMs containing different concentrations of dyes. (b) is the digital photos of FMs at 0.1 mg/mL (c) and (d) are the TEM images of D25 and T25, respectively. The scale bars at high magnification are 20 nm.

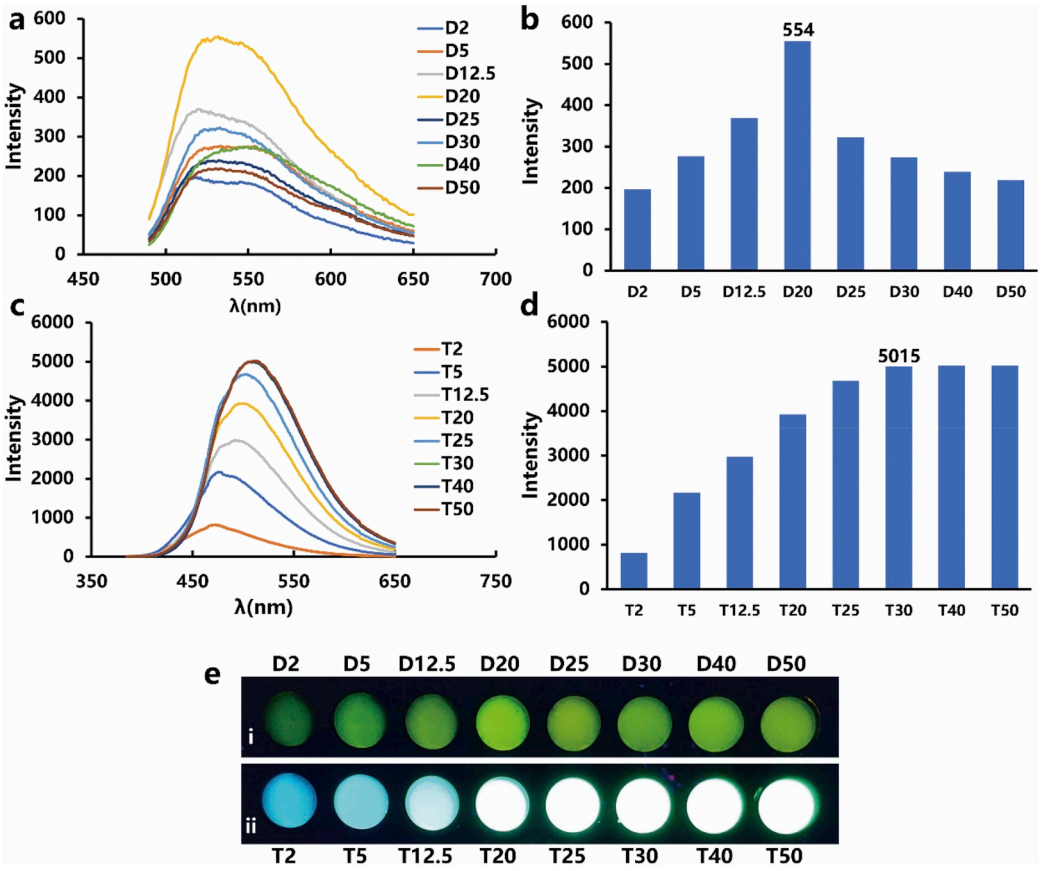

Fig. 3. Fluorescence intensity characterization of FMs (D2, 2 mg/mL DMF; D5, 5 mg/mL DMF; D12.5, 12.5 mg/mL DMF; D20, 20 mg/mL DMF; D25, 25 mg/mL DMF; D30, 30 mg/mL DMF; D40, 40 mg/mL DMF; D50, 50 mg/mL DMF; T2, 2 mg/mL TCBPE; T5, 5 mg/mL TCBPE; T12.5, 12.5 mg/mL TCBPE; T20, 20 mg/mL TCBPE; T25, 25 mg/mL TCBPE; T30, 30 mg/mL TCBPE; T40, 40 mg/mL TCBPE; T50, 50 mg/mL TCBPE). (a) Emission spectrum of DMFFMs with different concentrations of DMF under 470 nm excitation light; (b) corresponding histogram of maximum fluorescence intensity of DMFFMs, "554" is the maximum fluorescence intensity value of D20; (c) emission spectrum of AIEFMs with different concentrations at 365 nm excitation light; (d) corresponding histogram of the maximum fluorescence intensity of AIEFMs, "5015" is the maximum fluorescence intensity value of T30; (e) photos of DMFFMs in the dark under 470 nm excitation light (i), and AIEFMs in the dark with 365 nm excitation light (ii). The concentrations of DMFFMs and AIEFMs were 0.1 mg/mL.

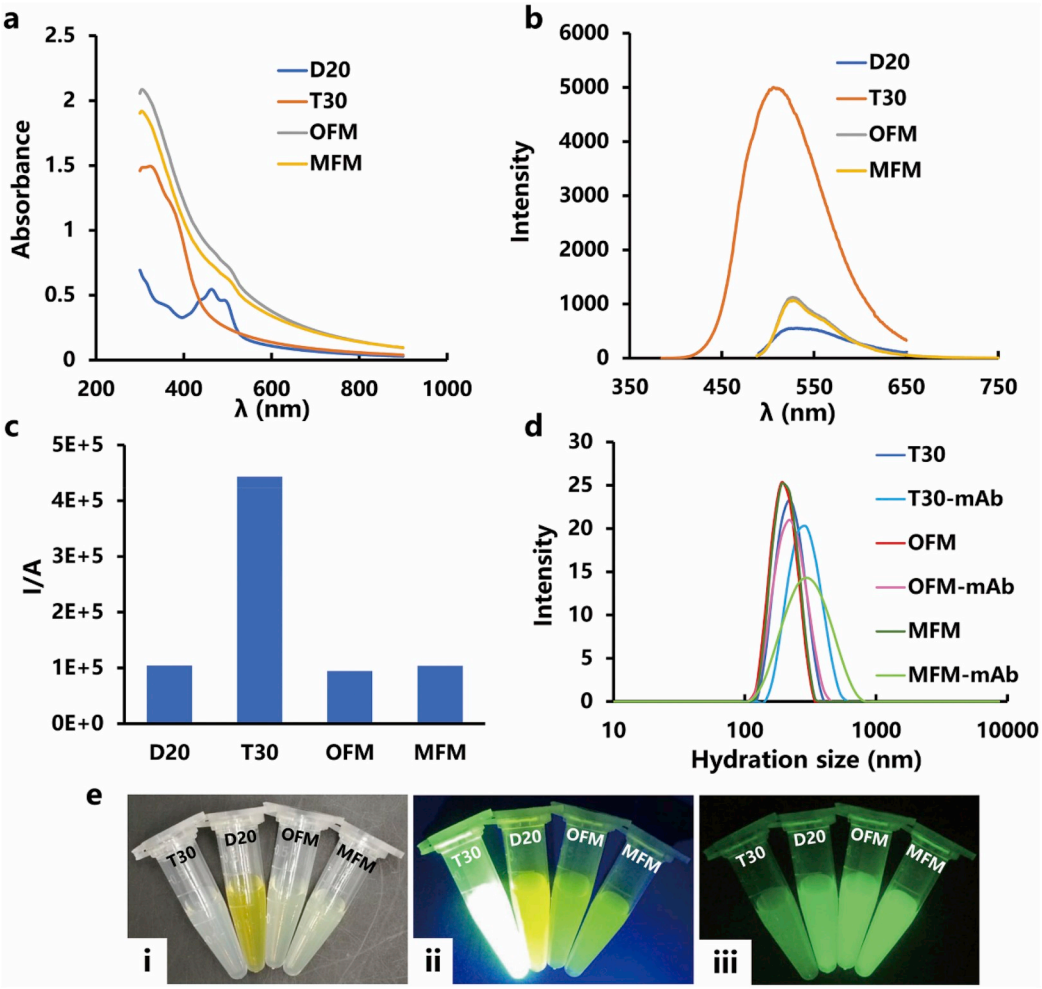

Fig. 4. Comparison of FMs. (a) UV–Vis spectrum of D20, T30, OFM, and MFM; (b) fluorescence emission spectrum of D20, T30, OFM, and MFM; (c) histogram of I/A (integral of fluorescence intensity/absorbance); (d) characterization of hydration size of T30, T30-mAb, OFM, OFM-mAb, MFM, and MFM-mAb; (e) digital photos of D20, T30, OFM, and MFM: (i) under the natural light; (ii) under UV light (365 nm); and (iii) under 470 nm excitation light. The concentrations of all of the dyes were 0.1 mg/mL.

25 (T25), 30 (T30), 40 (T40), and 50 mg/mL (T50) of TCBPE were 1.83×10^4, 2.25×10^4, 5.04×10^4, 6.80×10^4, 9.01×10^4, 1.07×10^5, and 1.19×10^5, respectively.

3.2. Comparison of FMs

The fluorescence intensity of FMs is the core performance as a probe in ICA and affected by different concentrations of loading dyes. Herein, we compared DMFFM and AIEFM made of DMF and TCBPE, respectively. The fluorescence intensities of DMFFM at 2 (D2), 5 (D5), 12.5 (D12.5), 20 (D20), 25 (D25), 30 (D30), 40 (D40), and 50 mg/mL (D50) of DMF were 196, 277, 369, 554, 322, 273, 239, and 219, respectively (Fig. 3a and Fig. 3b). The fluorescence intensity of DMFFM initially increased and decreased as the concentrations of loading DMF increased because of the ACQ effect. The fluorescence intensities of AIEFM at 2 (T2), 5 (T5), 12.5 (T12.5), 20 (T20), 25 (T25), 30 (T30), 40 (T40), and 50 mg/mL (T50) of TCBPE were 811.3, 2172, 2976, 3925, 4678, 5015, 5015, and 5018, respectively (Fig. 3c and d). The fluorescence intensity of AIEFM increased as the concentrations of loading TCBPE increased and retained a high value, indicating the absence of ACQ effect. The fluorescence intensity of AIEFM at 30 mg/mL of TCBPE (T30, 5015) was approximately 9 times higher than that of DMFFM at 20 mg/mL of DMF (D20, 554) because AIEFM could load more amounts of TCBPE without ACQ.

The emission spectrum of AIEFM with different concentrations and sizes was studied. By increasing concentration, the emission spectrum of AIEFM shifted from 472 to 512 nm (Fig. 3c), because the emission oscillators for TCBPE were coupled at large concentration. As shown in Fig. S4a and Fig. S4b, the hydration size of FMs was decreased with the increased of the power of ultrasonic processor. By increasing size, the emission spectrum of AIEFM shifted from 494 to 533 nm (Fig. S4d), while the emission spectrum of DMF stayed constant (525 nm, in Fig. S4c). These proved that the existence of AIE was based on the coherent coupling of emission dipoles.

Laser scanning confocal microscopy was conducted for characterization at the matching laser wavelength (for T30, 405 nm; for D20, 488 nm) with the same laser power (5%) and pinhole (1.00 AU) to compare the fluorescence property of the two FMs. In Fig. S5a and Fig. S5b, the fluorescence signal of T30 was significantly stronger than that of D20.

The Stokes' shift of TCBPE was larger than that of DMF (Fig. S1c and Fig. S1d). In the case of DMF, the significant overlap between emission and absorption spectra implies a significant homo-FRET and self-quenching. So, the fluorescence signal of AIEFM was significantly stronger than that of DMFFM (Fig. 3b and d).

Quantum yield (QY), which is the utilization of photons in photochemical reactions, is used as the key performance indicator of fluorescent probes. QY is calculated by measuring the fluorescence intensity in aqueous dispersion:

$Q_S = Q_R (I_S/I_R)\cdot(A_R/A_S)$ (Aboulaich et al., 2010),where Q_S is QY of

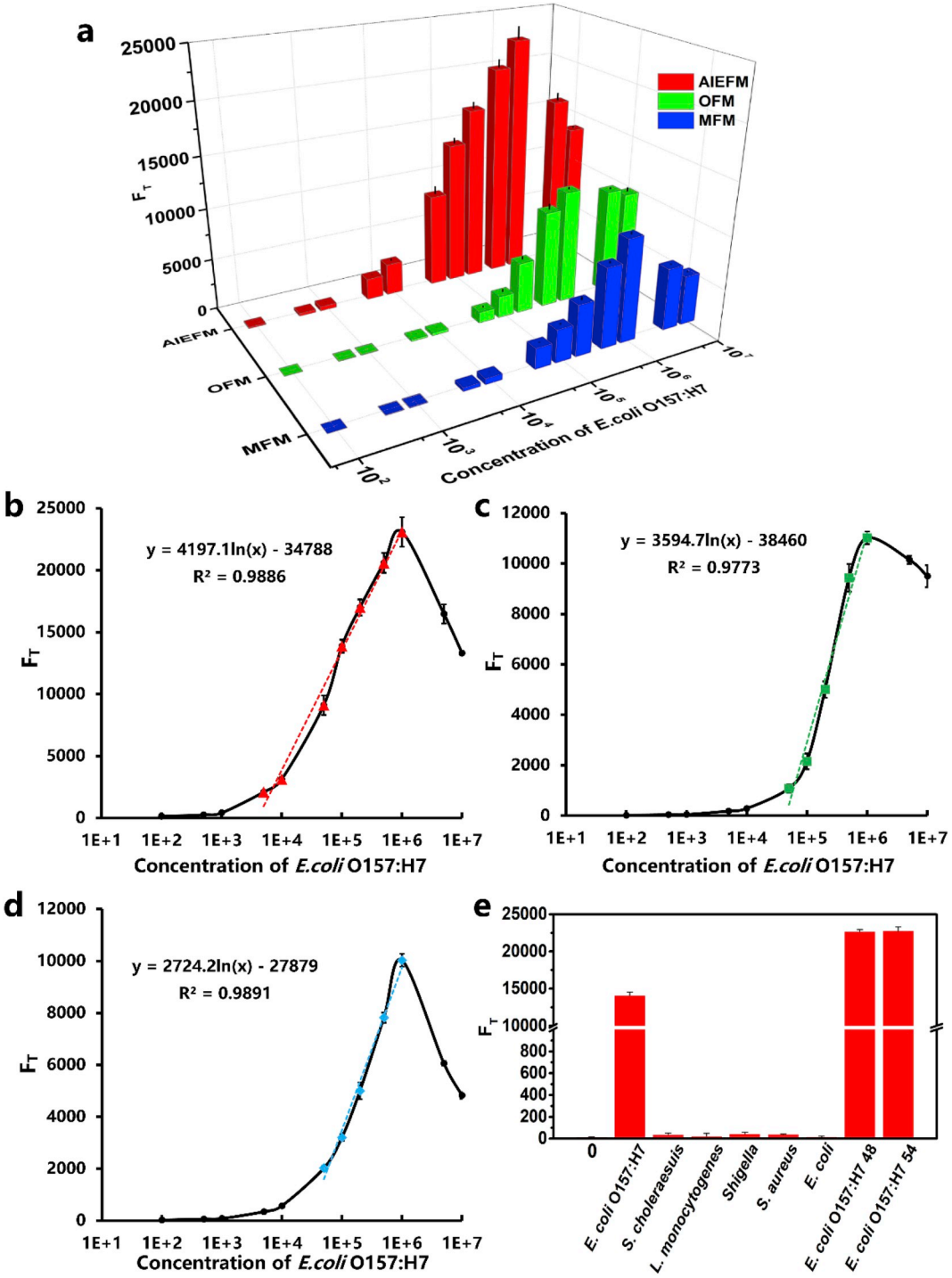

Fig. 5. Test results of ICA. (a) 3D histogram of ICA results. (b) Calibration curve of the ICA test strip for detecting *E. coli* O157:H7 based on AIEFM. (c) Calibration curve of the ICA test strip for detecting *E. coli* O157:H7 based on OFM. (d) Calibration curve of the ICA test strip for detecting *E. coli* O157:H7 based on MFM. (e) Specificity experiment of AIEFM-ICA. The concentration of *E. coli* O157:H7 (ATCC 43888) was 1×10^5 CFU/mL. The concentrations of *Salmonella choleraesuis* (*S. choleraesuis*), *Listeria monocytogenes* (*L. monocytogenes*), *Shigella*, *Staphylococcus aureus* (*S. aureus*), *Escherichia coli* (*E. coli*), *E. coli* O157:H7 48, and *E. coli* O157:H7 54, which were obtained from Jiangxi CDC, were 1×10^6 CFU/mL.

Table 1
Analytical characteristics of detection based on AIEFM, OFM, and MFM.

Probes	Linear range (CFU/mL)	LOD (CFU/mL)	Nonlinear fitting equation	R^2
AIEFM	5×10^3–1×10^6	3.98×10^3	y = 4197.1 ln(x) − 34788	0.9886
OFM	5×10^4–1×10^6	4.48×10^4	y = 3594.7 ln(x) − 38460	0.9799
MFM	5×10^4–1×10^6	2.78×10^4	y = 2724.2 ln(x) − 27879	0.9891

the sample, Q_R is QY of reference, I is the measured intensity of luminescent spectra, and A is the absorbance at the excitation wavelength. The absorption and fluorescence intensity of T30 ($\lambda_{excitation}$ = 365 nm, $\lambda_{emission}$ = 506 nm) were stronger than that of D20 ($\lambda_{excitation}$ = 470 nm, $\lambda_{emission}$ = 532 nm) (Fig. 4a and Fig. 4b). For the absorption and fluorescence intensity (Fig. 4c), QY of T30 ($I_{T30}/A_{T30} = 4.43 \times 10^5$) was approximately 4.5 times higher than that of D20 ($I_{D20}/A_{D20} = 1.04 \times 10^5$) by calculating with the following equation:

$$Q_{T30}/Q_{D20} = (I_{T30}/A_{T30})/(I_{D20}/A_{D20}).$$

Two commoditized FMs obtained from Ocean (OFM) and Merk (MFM) were utilized as comparison. In Fig. 4b and Fig. S4, the maximum fluorescence intensity of AIEFM (5015) was approximately five times higher than those of OFM (1124) and MFM (1070). In addition, the relative QY of AIEFM was 4.5 times higher than those of OFM ($I_{OFM}/A_{OFM} = 9.46 \times 10^4$) and MFM ($I_{MFM}/A_{MFM} = 1.04 \times 10^5$) (as shown in Fig. 4c). These results indicated that AIEFM (T30) had the most superior optical performance.

3.3. Utilization in immunochromatographic assay

The AIEFM (T30) and the two commoditized FMs (OFM and MFM) were utilized in ICA for the detection of *E. coli* O157:H7. Three immune probes (T30-mAb, OFM-mAb, and MFM-mAb) were prepared by 1-ethyl-3-(3-dimethylaminopropyl) carbodiimide/*N*-hydroxysulfosuccinimide sodium (EDC/NHS) assay (Keleştemur et al., 2017). In Fig. 4d, the hydration size of T30, OFM, and MFM with mAb binding increased 55.4, 19.8, and 74.7 nm, respectively, indicating that the antibody was successfully bound to the FMs.

Serially spiked samples were detected by using an ICA test strip to establish the calibration curve (Fig. 5a, Fig. 5b and 5c). The calibration curve was constructed by plotting the fluorescent intensity of T (F_T) as the ordinate (Y) and the concentrations of *E. coli* O157:H7 as the abscissa (X). The detection curves exhibited good linearity, and the coefficient of variation was less than 9.97% at each concentration (The coefficient of variation was less than 8.59%, Table S2). The limit of detection (LOD) was calculated by finding the concentration at which the signal-to-noise ratio was three (S/N = 3) (Xu et al., 2009). The nonlinear fitting equation and the LOD are listed in Table 1. The photos under UV light are shown in Fig. S6.

As a result, the LOD of ICA based on AIEFM was 3.98×10^3 CFU/mL, and the LODs of ICA based on OFM and MFM were 4.48×10^4 and 2.78×10^4 CFU/mL, respectively. The sensitivity of ICA based on AIEFM was 11 and 7 times higher than that based on OFM and MFM. We think it is because AIEFM had the advantage of optical performance in Stokes' shift, fluorescence intensity, and QY. In this experiment, the signal intensity increased with the concentrations of *E. coli* O157:H7 from 0 to 1×10^6 CFU/mL but subsequently decreased at higher concentrations in the test line. This phenomenon, called the Hook effect (Oh et al., 2014), often occurred in immunoassays with high-concentration targets.

The result of the specificity experiment is shown in Fig. 5d and Fig. S6d. The ICA test strips provided consistent positive results with *E. coli* O157:H7 (1×10^5 CFU/mL) stored in our lab and two locale isolated *E. coli* O157:H7 (1×10^6 CFU/mL) from Jiangxi CDC, and negative results with *Salmonella choleraesuis* (1×10^6 CFU/mL), *Listeria monocytogenes* (1×10^6 CFU/mL), *Shigella* (1×10^6 CFU/mL), *Staphylococcus aureus* (1×10^6 CFU/mL), and *E. coli* (1×10^6 CFU/mL), indicating that ICA based on AIEFM had excellent specificity.

4. Conclusion

In conclusion, AIEFM was synthesized and systematically compared with conventional FMs. AIEFM had larger Stokes' shift, better fluorescence intensity and higher relative QY compared with those of conventional FMs. The results show the AIEFM has a bright prospect in many areas. In this work, the AIEFM was firstly used as probe for improving the sensitivity of ICA. The ICA of AIEFM had order of magnitude improvement in sensitivity compared with that of two commercial FMs. Our study provide a new strategy to guide the design of novel AIE probe in ICA.

Declaration of interests

The authors declare that they have no known competing financial interests or personal relationships that could have appeared to influence the work reported in this paper.

The authors declare the following financial interests/personal relationships which may be considered as potential competing interests.

CRediT authorship contribution statement

Gang-gang Zhang: Conceptualization, Methodology, Software, Data curation, Writing - original draft. **Shao-lan Xu:** Methodology, Software, Data curation. **Yong-hua Xiong:** Conceptualization. **Hong Duan:** Investigation, Resources. **Wen-yao Chen:** Data curation. **Xiang-min Li:** Investigation. **Mei-fang Yuan:** Validation. **Wei-hua Lai:** Conceptualization, Writing - review & editing, Supervision, Project administration, Funding acquisition.

Acknowledgement

This work was supported by the National Natural Science Foundation of China (No. 31772066), the Open Project Program of State Key Laboratory of Food Science and Technology, Nanchang University (No. SKLF-KF-201616), Jiangxi earmarked fund for Jiangxi Agriculture Research System (JXARS-03).

Appendix A. Supplementary data

Supplementary data related to this article can be found at https://doi.org/10.1016/j.bios.2019.04.023.

References

Aboulaich, A., Geszke, M., Balan, L., Ghanbaja, J., Medjahdi, G., Schneider, R., 2010. Inorg. Chem. 49 (23), 10940–10948.
Bishnoi, S.W., Lin, Y.J., Tibudan, M., Huang, Y., Nakaema, M., Swarup, V., Keiderling, T.A., 2011. Anal. Chem. 83 (11), 4053–4060.
Chen, J., Law, C.C.W., Lam, J.W.Y., Dong, Y., Lo, S.M.F., Williams, I.D., Zhu, D., Tang, B.Z., 2003. Chem. Mater. 15 (7), 1535–1546.
Chen, J., Zhang, P., Fang, G., Yi, P., Yu, X., Li, X., Zeng, F., Wu, S., 2011. J. Phys. Chem. B 115 (13), 3354–3362.
Chen, G., Li, W., Zhou, T., Peng, Q., Zhai, D., Li, H., Yuan, W.Z., Zhang, Y., Tang, B.Z., 2015. Adv. Mater. 27 (30), 4496–4501.
Chen, S., Wang, H., Hong, Y., Tang, B.Z., 2016. Mater. Horiz. 3 (4), 283–293.
Chen, Y., Guo, L., Liu, L., Song, S., Kuang, H., Xu, C., 2017. J. Agric. Food Chem. 65 (37), 8248–8255.
Duan, H., Huang, X., Shao, Y., Zheng, L., Guo, L., Xiong, Y., 2017. Anal. Chem. 89 (13), 7062–7068.
Feng, S., Caire, R., Cortazar, B., Turan, M., Wong, A., Ozcan, A., 2014. ACS Nano 8 (3), 3069–3079.
Fu, B., Huang, J., Bai, D., Xie, Y., Wang, Y., Wang, S., Zhou, X., 2015. Chem. Commun. 51 (95), 16960–16963.
Gong, X., Cai, J., Zhang, B., Zhao, Q., Piao, J., Peng, W., Gao, W., Zhou, D., Zhao, M., Chang, J., 2017. J. Mater. Chem. B 5 (26), 5079–5091.
Haruo, O., Youko, I., Teiji, C., Shousuke, T., Kazuo, T., 1986. Bull. Chem. Soc. Jpn. 59 (8), 2481–2483.
He, H., Liu, B., Wen, S., Liao, J., Lin, G., Zhou, J., Jin, D., 2018a. Anal. Chem. 90 (21), 12356–12360.
He, T., Niu, N., Chen, Z., Li, S., Liu, S., Li, J., 2018b. Adv. Funct. Mater. 28 (11), 1870068.
Hu, J., Wang, L., Li, F., Han, Y.L., Lin, M., Lu, T.J., Xu, F., 2013. Lab Chip 13 (22), 4352–4357.
Hu, L.M., Luo, K., Xia, J., Xu, G.M., Wu, C.H., Han, J.J., Zhang, G.G., Liu, M., Lai, W.H., 2017. Biosens. Bioelectron. 91, 95–103.
Huang, M., Yu, R., Xu, K., Ye, S., Kuang, S., Zhu, X., Wan, Y., 2016. Chem. Sci. 7 (7), 4485–4491.
Keleştemur, S., Altunbek, M., Culha, M., 2017. Appl. Surf. Sci. 403, 455–463.

Kim, S., Fujitsuka, M., Tohnai, N., Tachikawa, T., Hisaki, I., Miyata, M., Majima, T., 2015. Chem. Commun. 51 (58), 11580–11583.
Kong, D., Liu, L., Song, S., Suryoprabowo, S., Li, A., Kuang, H., Wang, L., Xu, C., 2016. Nanoscale 8 (9), 5245–5253.
Li, D., Qin, W., Xu, B., Qian, J., Tang, B.Z., 2017. Adv. Mater. 29 (43), 1703643.
Li, G., Wang, D., Zhou, A., Sun, Y., Zhang, Q., Poapolathep, A., Zhang, L., Fan, Z., Zhang, Z., Li, P., 2018. J. Agric. Food Chem. 66 (22), 5671–5676.
Liu, D., Huang, Y., Chen, M., Wang, S., Liu, K., Lai, W., 2015. Food Control 50, 659–662.
Liu, B., Nie, H., Zhou, X., Hu, S., Luo, D., Gao, D., Zou, J., Xu, M., Wang, L., Zhao, Z., Qin, A., Peng, J., Ning, H., Cao, Y., Tang, B.Z., 2016. Adv. Funct. Mater. 26 (5), 776–783.
Lou, D., Fan, L., Cui, Y., Zhu, Y., Gu, N., Zhang, Y., 2018. Anal. Chem. 90 (11), 6502–6508.
Loynachan, C.N., Thomas, M.R., Gray, E.R., Richards, D.A., Kim, J., Miller, B.S., Brookes, J.C., Agarwal, S., Chudasama, V., Mckendry, R.A., 2018. ACS Nano 12 (1), 279–288.
Lu, H., Zheng, Y., Zhao, X., Wang, L., Ma, S., Han, X., Xu, B., Tian, W., Gao, H., 2016. Angew. Chem. Int. Ed. 55 (1), 155–159.
Maji, S., Alam, P., Kumar, G.S., Biswas, S., Sarkar, P.K., Das, B., Rehman, I., Das, B.B., Jana, N.R., Laskar, I.R., Acharya, S., 2017. Small 13 (15), 1603780.
Mei, J., Hong, Y., Lam, J.W., Qin, A., Tang, Y., Tang, B.Z., 2014. Adv. Mater. 26 (31), 5429–5479.
Nie, H., Chen, B., Zeng, J., Xiong, Y., Zhao, Z., Tang, B.Z., 2018. J. Mater. Chem. C 6 (14), 3690–3698.
Oh, Y.K., Joung, H.A., Han, H.S., Suk, H.J., Kim, M.G., 2014. Biosens. Bioelectron. 61, 285–289.
Ouyang, H., Tu, X., Fu, Z., Wang, W., Fu, S., Zhu, C., Du, D., Lin, Y., 2018. Biosens. Bioelectron. 106, 43–49.
Parolo, C., Merkoci, A., 2013. Chem. Soc. Rev. 42 (2), 450–457.
Qiao, B., Li, Y., Hu, P., Sun, Y., Si, Z., Lu, S., Ren, H., Liu, Z., Zhang, Y., Meng, L., 2018. Sensor. Actuator. B Chem. 262.
Qiu, T., Chen, Y., Song, J., Fan, L.-J., 2015. ACS Appl. Mater. Interfaces 7 (15), 8260–8267.
Reisch, A., Klymchenko, A.S., 2016. Small 12 (15), 1968–1992.
Ren, M., Xu, H., Huang, X., Kuang, M., Xiong, Y., Xu, H., Xu, Y., Chen, H., Wang, A., 2014. ACS Appl. Mater. Interfaces 6 (16), 14215–14222.
Shan, S., Lai, W., Xiong, Y., Wei, H., Xu, H., 2015. J. Agric. Food Chem. 63 (3), 745–753.
Shao, Y., Duan, H., Guo, L., Leng, Y., Lai, W., Xiong, Y., 2018. Anal. Chim. Acta 1025, 163–171.
Tang, X., Li, P., Zhang, Q., Zhang, Z., Zhang, W., Jiang, J., 2017. Anal. Chem. 89 (21), 11520–11528.
Wang, D.B., Tian, B., Zhang, Z.P., Wang, X.Y., Fleming, J., Bi, L.J., Yang, R.F., Zhang, X.E., 2015. Biosens. Bioelectron. 67, 608–614.
Wang, W., Liu, L., Xu, L., Kuang, H., Zhu, J., Xu, C., 2016. Part. Part. Syst. Char. 33 (7), 388–395.
Wu, Z., Shen, H., Hu, J., Fu, Q., Yao, C., Yu, S., Xiao, W., Tang, Y., 2017. Anal. Bioanal. Chem. 409 (22), 5209–5216.
Xiao, M., Fu, Q., Shen, H., Chen, Y., Xiao, W., Yan, D., Tang, X., Zhong, Z., Tang, Y., 2017. Talanta 178, 644–649.
Xie, Q.Y., Wu, Y.H., Xiong, Q.R., Xu, H.Y., Xiong, Y.H., Liu, K., Jin, Y., Lai, W.H., 2014. Biosens. Bioelectron. 54, 262–265.
Xu, H., Mao, X., Zeng, Q., Wang, S., Kawde, A.-N., Liu, G., 2009. Anal. Chem. 81 (2), 669–675.
Yan, L., Zhang, Y., Xu, B., Tian, W., 2016. Nanoscale 8 (5), 2471–2487.
Yang, Z., Qin, W., Leung, N.L.C., Arseneault, M., Lam, J.W.Y., Liang, G., Sung, H.H.Y., Williams, I.D., Tang, B.Z., 2016. J. Mater. Chem. C 4 (1), 99–107.
You, M., Lin, M., Gong, Y., Wang, S., Li, A., Ji, L., Zhao, H., Ling, K., Wen, T., Huang, Y., Gao, D., Ma, Q., Wang, T., Ma, A., Li, X., Xu, F., 2017. ACS Nano 11 (6), 6261–6270.
Zhao, Z., He, B., Tang, B.Z., 2015. Chem. Sci. 6 (10), 5347–5365.
Zhou, J., Zhu, K., Xu, F., Wang, W., Jiang, H., Wang, Z., Ding, S., 2014. J. Agric. Food Chem. 62 (49), 12061–12066.